AD

TECHNICAL REPORT ARBRL-TR-02515

(Supersedes IMR No. 745)

COMPUTATIONS OF PROJECTILE MAGNUS EFFECT

AT TRANSONIC VELOCITIES

Charles J. Nietubicz
Walter B. Sturek
Karen R. Heavey

TECHNICAL
LIBRARY

August 1983

US ARMY ARMAMENT RESEARCH AND DEVELOPMENT COMMAND
BALLISTIC RESEARCH LABORATORY
ABERDEEN PROVING GROUND, MARYLAND

REPORT DOCUMENTATION PAGE		READ INSTRUCTIONS BEFORE COMPLETING FORM
1. REPORT NUMBER TECHNICAL REPORT ARBRL-TR-02515	2. GOVT ACCESSION NO.	3. RECIPIENT'S CATALOG NUMBER
4. TITLE *(and Subtitle)* COMPUTATIONS OF PROJECTILE MAGNUS EFFECT AT TRANSONIC VELOCITIES		5. TYPE OF REPORT & PERIOD COVERED Final
		6. PERFORMING ORG. REPORT NUMBER
7. AUTHOR(s) C.J. Nietubicz, W.B. Sturek, and K.R. Heavey		8. CONTRACT OR GRANT NUMBER(s)
9. PERFORMING ORGANIZATION NAME AND ADDRESS U.S. Army Ballistic Research Laboratory ATTN: DRDAR-BLL Aberdeen Proving Ground, Maryland 21005		10. PROGRAM ELEMENT, PROJECT, TASK AREA & WORK UNIT NUMBERS RDT&E 1L161102AH43
11. CONTROLLING OFFICE NAME AND ADDRESS US Army Armament Research & Development Command US Army Ballistic Research Laboratory (DRDAR-BLA-S) Aberdeen Proving Ground, MD 21005		12. REPORT DATE August 1983
		13. NUMBER OF PAGES 32
14. MONITORING AGENCY NAME & ADDRESS*(If different from Controlling Office)*		15. SECURITY CLASS. *(of this report)* UNCLASSIFIED
		15a. DECLASSIFICATION/DOWNGRADING SCHEDULE

16. DISTRIBUTION STATEMENT *(of this Report)*

Approved for public release, distribution unlimited.

17. DISTRIBUTION STATEMENT *(of the abstract entered in Block 20, if different from Report)*

18. SUPPLEMENTARY NOTES

This report supersedes IMR No. 745

19. KEY WORDS *(Continue on reverse side if necessary and identify by block number)*

Transonic Flow   Projectile Aerodynamics
Magnus Effect
Computational Methods
Implicit Scheme
Navier-Stokes Solver

20. ABSTRACT *(Continue on reverse side if necessary and identify by block number)*

The Magnus effect has long been the nemesis of shell designers. Although very small in magnitude, on the order of 1/10th the normal force, this spin-induced side moment has a significant destabilizing effect on projectiles. A combined computational and experimental research program has been ongoing at BRL in recent years to develop a predictive capability for the Magnus effect in particular and for projectile aerodynamics in general. This effort has been very successful in the supersonic regime. The research to be reported in this paper is an extension of this effort into the transonic regime. Utiliz-

DD ~~FORM~~ 1_{JAN 73} **1473**   EDITION OF 1 NOV 65 IS OBSOLETE

20. ABSTRACT (Continued)

ing the time marching, thin-layer Navier-Stokes computational technique developed at NASA Ames Research Center, solutions have been obtained for a spinning, 6-caliber long, ogive-cylinder-boattail shape at Mach = 0.91 and angle of attack = 2°. The computed results predict the correct development of the Magnus force along the body, and comparisons between the computation and experiment are very favorable. Details of the flow field solution such as turbulent boundary-layer velocity profiles and surface pressure distributions are presented. The components which contribute to the Magnus effect are determined and presented as a function of axial position. A complete set of aerodynamic coefficients have been determined from the flow field solutions. Those to be presented here and compared with experimental data include the normal force and Magnus force coefficients. The computations for this research effort were obtained both on a CDC 7600 computer and Cray 1S. The results of this research effort provide the first computations of the Magnus effect at transonic velocity and represent a significant new computational capability for predicting the aeroballistics of shell.

TABLE OF CONTENTS

LIST OF ILLUSTRATIONS

I. INTRODUCTION

The accurate prediction or experimental determination of projectile aerodynamics is of significant importance to the shell designer and ballistician. The shell designer requires accurate aerodynamic data for the overall development of new shell. The ballistician is concerned with the development of aiming data and therefore relies heavily on accurate aerodynamic data. Experimental costs have skyrocketed in recent years and have contributed significantly to overall system development costs. Computational techniques are beginning to show promise as a means to alleviate or at least temper these rising development costs by providing relatively low cost computer analysis of new designs. As computer technology increases and machines become faster with larger memory, the use of computational methods in design becomes more of a reality.

The means to compute projectile aerodynamics for all Mach number regimes covered by a given projectile in its flight history has been an area of research actively pursued by the Aerodynamics Research Branch of the Ballistic Research Laboratory. Early work had focused on the supersonic flight regime and, in particular, on the accurate prediction of the Magnus force. The Magnus force, which is very small in magnitude (on the order of 1/10 the normal force), is a critical parameter in determining the dynamic stability of shell. The Magnus force is generated by a spin-induced distortion of the boundary layer; therefore, correct modeling of the viscous/inviscid interation is critical for accurate computations. The work of Sturek et. al.[1] has shown that accurate results in the supersonic regime can be obtained for ogive-cylinder projectile shapes. This technique involved separate computations of the turbulent, viscous boundary layer and the outer inviscid flow field. As the projectile shapes were generalized to include boattails, more sophisticated computational techniques had to be employed. These new methods, which solved the thin-layer Navier Stokes equations, were successfully applied to ogive-cylinder-boattail shapes by Sturek and Schiff.[2,3] The solution of the Navier-Stokes equations allows for the simultaneous computation of the viscous/inviscid flow field and thus provided the basis for good Magnus force prediction.

---

1. Sturek, W.B., et al., "Computations of Magnus Effects for a Yawed, Spinning Body of Revolution," *AIAA Journal*, Vol. 16, No. 7, July 1978, pp. 687-692.

2. Schiff, L.B., and Sturek, W.B., "Numerical Simulation of Steady Supersonic Flow Over Cone Ogive-Cylinder-Boattail Body," AIAA Paper No. 80-0066, January 14-16, 1980; also, ARBRL-TR-02363, U.S. Army Ballistic Research Laboratory, ARRADCOM, Aberdeen Proving Ground, MD 21005, September 1981 (AD A106060).

3. Sturek, W.B., and Schiff, L.B., "Computations of the Magnus Effect for Slender Bodies in Supersonic Flow," *AIAA Journal*, Vol. 20, No. 12, December 1982, pp. 1724-1731.

A region of critical aerodynamic behavior occurs in the transonic regime, $0.90 < M < 1.15$, where aerodynamic coefficients have been found to increase by as much as 100%. This flight velocity regime is both experimentally and computationally difficult. Thus, only a small amount of experimental data are available for design studies and only limited computational studies have been made. An initial attempt to develop a computational capability suitable for Magnus prediction at transonic velocity was made by Nietubicz, et. al[4] whereby the thin-layer Navier Stokes computational technique was applied to standard and hollow projectile shapes at zero degrees angle of attack. Computational results were also obtained for non-spinning projectiles at angle of attack;[5] however, limitations of computer resources (CDC 7600) became apparent. The computational results obtained by Deiwert,[6] on the ILLIAC IV, indicating the complicated flow pattern which exists on a boattailed afterbody, demonstrates the capability of the Navier-Stokes codes given sufficient computer resources. In this paper, recent results are presented for Magnus force computations using the Cray 1S computer. Comparisons are made with earlier CDC computer results and are further compared to some limited experimental data. A brief discussion of the numerical technique is included.

II. GOVERNING EQUATIONS AND COMPUTATIONAL TECHNIQUE

The Navier-Stokes equations solved here make use of the thin-layer approximation.[7] That is, the viscous terms are neglected in both the longitudinal and circumferential directions. The viscous terms are retained, however, in a direction nearly normal to the surface where large flow field gradients exist. This formulation retains the momentum equations in all three coordinate directions. The retention of the three momentum equations allows for the computation of separated flow and thus differs significantly from boundary layer assumptions.

The equations solved here are written in a generalized coordinate system. This allows a wide variety of body shapes to be computed using the same basic numerical technique. The notation for the physical and transformed coordinate

4.   Nietubicz, C.J., Pulliam, T.H., and Steger, J.L., "Numerical Solution of the Azimuthal-Invariant Thin-Layer Navier-Stokes Equations," *AIAA Journal*, Vol. 18, No. 12, December 1980, pp. 1411-1412.

5.   Nietubicz, C.J., "Navier-Stokes Computations for Conventional and Hollow Projectile Shapes at Transonic Velocities," AIAA Paper No. 81-1262, AIAA 14th Fluid and Plasma Dynamics Conference, Palto Alto, CA, 1981; also, ARBRL-MR-03184, U.S. Army Ballistic Research Laboratory, ARRADCOM, Aberdeen Proving Ground, MD 21005, July 1982 (AD A116866).

6.   Deiwert, G.S., "Numerical Simulation of Three Dimensional Boattail Afterbody Flow Field," *AIAA Journal*, Vol. 19, No. 5, May 1981, pp. 582-588.

7.   Baldwin, B.S., and Lomax, H., "Thin Layer Approximation and Algebraic Model for Separated Turbulent Flows," AIAA Paper No. 78-257, January 1978.

systems are shown in Figure 1. The three-dimensional, transformed, thin-layer Navier-Stokes equations, written in nondimensional, strong conservation law form are[8]

$$\partial_\tau \hat{q} + \partial_\xi \hat{E} + \partial_\eta \hat{F} + \partial_\zeta \hat{G} = Re^{-1} \partial_\zeta \hat{S} \tag{1}$$

The general coordinate transformations are defined as

$\xi = \xi(x,y,z,t)$ — longitudinal coordinate

$\eta = \eta(x,y,z,t)$ — circumferential coordinate

$\zeta = \zeta(x,y,z,t)$ — near Normal coordinate

$\tau = t$ — time

and

$$\hat{q} = J^{-1} \begin{bmatrix} \rho \\ \rho u \\ \rho v \\ \rho w \\ e \end{bmatrix} \qquad \hat{E} = J^{-1} \begin{bmatrix} \rho U \\ \rho u U + \xi_x p \\ \rho v U + \xi_y p \\ \rho w U + \xi_z p \\ (e+p)U - \xi_t p \end{bmatrix}$$

$$\hat{F} = J^{-1} \begin{bmatrix} \rho V \\ \rho u V + \eta_x p \\ \rho v V + \eta_y p \\ \rho w V + \eta_z p \\ (e+p)V - \eta_t p \end{bmatrix} \qquad \hat{G} = J^{-1} \begin{bmatrix} \rho W \\ \rho u W + \zeta_x p \\ \rho v W + \zeta_y p \\ \rho w W + \zeta_z p \\ (e+p)W - \zeta_t p \end{bmatrix}$$

The viscous matrix, $\hat{S}$, is written as

8. Pulliam, T.H., and Steger, J.L., "On Implicit Finite-Difference Simulations of Three-Dimensional Flow," AIAA Journal, Vol. 18, No. 2. February 1980, pp. 159-167.

$$\hat{S} = J^{-1} \begin{bmatrix} 0 \\[4pt] \mu(\zeta_x^2+\zeta_y^2+\zeta_z^2)u_\zeta+(\mu/3)(\zeta_x u_\zeta+\zeta_y v_\zeta+\zeta_z w_\zeta)\zeta_x \\[4pt] \mu(\zeta_x^2+\zeta_y^2+\zeta_z^2)v_\zeta+(\mu/3)(\zeta_x u_\zeta+\zeta_y v_\zeta+\zeta_z w_\zeta)\zeta_y \\[4pt] \mu(\zeta_x^2+\zeta_y^2+\zeta_z^2)w_\zeta+(\mu/3)(\zeta_x u_\zeta+\zeta_y v_\zeta+\zeta_z w_\zeta)\zeta_z \\[4pt] \{(\zeta_x^2+\zeta_y^2+\zeta_z^2)[\mu/2(u^2+v^2+w^2)_\zeta+\kappa Pr^{-1}(\gamma-1)^{-1}(a^2)_\zeta] \\[4pt] +(\mu/3)(\zeta_x u+\zeta_y v+\zeta_z w)(\zeta_x u_\zeta+\zeta_y v_\zeta+\zeta_z w_\zeta)\} \end{bmatrix}$$

The velocities

$$U = \xi_t + \xi_x u + \xi_y v + \xi_z w$$
$$V = n_t + n_x u + n_y v + n_z w \qquad\qquad (2)$$
$$W = \zeta_t + \zeta_x u + \zeta_y v + \zeta_z w$$

represent the contravarient velocities. The nondimensional velocities U, V, and W are those components in the direction of the transformed coordinates ξ, n, and ζ, respectively. The Cartesian velocity components u, v, w together with the density ρ and total energy per unit volume e are retained as the dependent variables. The local pressure, p, is determined using the relation

$$p = (\gamma - 1)(e - .5\rho(u^2 + v^2 + w^2)).$$

The velocities are nondimensionalized by the free-stream speed of sound a_∞, the density by ρ_∞, and the total energy by $\rho_\infty a_\infty^2$. The additional parameters appearing in equation 1 are: (a) coefficient of thermal conductivity, κ; (b) dynamic viscosity, μ; (c) Reynolds number based on body diameter, Re; (d) Prandtl number, Pr.

As mentioned earlier, these equations are written in transformed coordinates; therefore, the various body shapes are introduced through determination of the metric terms ξ_x, n_x, ζ_z, etc. These terms are formed by a combination of the derivative terms x_ζ, y_ζ, z_ζ, etc., and, together with the transformation Jacobian, allow for variable body geometries. Thus, one of the first steps in performing a computation is the generation of a computational grid which provides the x, y, z points for the metric determination. These points are determined prior to the computations and are not changed with time. Examples of the computational grid used in this study are shown in Figures 2 and 3. A two-dimensional slice of the overall grid is shown in Figure 2. The

10

upstream, downstream and outer flow field computational boundaries extended approximately 18 body diameters from the body surface. At this distance the flow field should be uniform and the imposed boundary conditions are considered valid. Figure 3 shows an expanded view near the body. The clustering of grid points near the body surface is required in order to resolve the viscous components of the flow field near the body surface. Due to the lack of sufficient computer storage, judicious use must be made of the limited grid points available. In regions where the viscous effects are not predominant and the flow field changes slowly, the grid points are sparse. Additional grid clustering is used in the longitudinal direction where flow field gradients are expected. The two-dimensional grid shown in Figure 2 was rotated about the body axis in 10-degree increments for the Cray computations (20-degree increments for the CDC 7600) in order to obtain the three-dimensional grid required for computations at angle of attack. The wake was modeled by extending the boattail for approximately two calibers $(X/D = 7.8)$, turning the grid line parallel to the model axis and extending it to the downstream boundary.

As mentioned in the introduction, the Magnus effect is produced by a spin induced distortion of the boundary layer. The computation must therefore be fully three-dimensional since no plane of symmetry exists. The boundary conditions used for the computations are:

(1) inner boundary, body surface

$$U = W = 0$$
$$V = \frac{\omega D}{2 a_\infty}$$

ρ - first order extrapolation
p - calculated using the three transformed momentum
    equations

(2) outer boundary

constant free stream values are used for all variables

(3) downstream boundary

$M < 1$ pressure is fixed at p_∞ and all other variables
                 are extrapolated
$M \geqslant 1$ first order extrapolation on all variables

The numerical scheme used for the solution of Equation 1 is a fully implicit, approximately factored, finite difference algorithm in delta form as analyzed by Beam and Warming.[9] This scheme can be first or second order accurate in time and second or fourth order accurate in the three spatial

9. Beam, R., and Warming, R.F., "An Implicit Factored Scheme for the Compressible Navier-Stokes Equations," AIAA Journal, Vol. 16, No. 4, April 1978, pp. 393-402.

4.5×10^6. The Magnus measurements were compared for a nondimensional spin parameter, $PD/V = 0.39$ where P = angular velocity, D = maximum body diameter and V = free-stream velocity. Surface pressure comparisons are made using the Langley data, while the aerodynamic coefficient comparisons are made with the NSWC data.[12]

A. Surface Pressure Coefficient

The surface pressure coefficient, C_p on the leeward ray is shown as a function of longitudinal position in Figure 5. The experimental data, and computational results from both the CDC 7600 and Cray 1S computers are shown. The CDC results (dashed line) show marginal agreement with the experimental data (circles) over the entire projectile surface. The expansions and recompressions which occur near the ogive-cylinder and cylinder-boattail junction have not been adequately captured by the computation. The solid line in Figure 5 is the result from the computation on the Cray 1S computer where the grid has been expanded. The agreement with the experimental data has improved significantly. Some discrepancy is still apparent, however, on the cylinder and on the boattail. As can be seen from Figure 3 the grid points in the vicinity of the boattail have been severely stretched and is the apparent cause of the discrepancy. All remaining results to be presented were obtained from the Cray 1S. A comparison of the windward and leeward pressure distribution is shown in Figure 6. The ogive experiences high pressure along the windward side whereas the high pressure for the boattail is on the leeward side. This condition forms a couple about the center of gravity and contributes to the critical aerodynamic behaviour which occurs at transonic velocities.

Comparisons between computation and experiment for the circumferential surface pressure distribution are shown in Figures 7 and 8 for X/D stations 1.56 and 5.19, respectively. As seen in these figures, the computation predicts the correct trend of the data while the actual magnitude shows a deviation. Upon close evaluation of the circumferential pressure distribution, a slight asymmetry is detected about the $\phi = 180$ plane. This condition contributes to the expected side force. The grid used for these calculations is by no means optimum and additional computational experimentation is required. The results do, however, indicate the potential for obtaining satisfactory aerodynamic coefficients. This optimism is based on results which have been obtained[5] previously for an axisymmetric computation. Figure 9 shows a comparison between experimental data and a computation using a grid consisting of 80 longitudinal points and 40 points in the near normal direction. The agreement is excellent and indicates the quality of results which should be possible for the three-dimensional cases when adequate grid resolution is achieved.

A primary purpose of this research effort is the development of a capability for the prediction of aerodynamic coefficients and, in particular, the

---

12. Kayser, L.D., Ballistic Research Laboratory/ARRADCOM, Aberdeen Proving Ground, Maryland 21005, private communications.

14

capability to compute the Magnus effect. As noted, the Magnus effect is a viscous phenonena associated with the spinning projectile. Therefore, in order for a computational technique to predict this effect, it must adequately compute the longitudinal and circumferential wall shear stress for the spinning projectile at angle of attack. The experimental determination of the u, v, and w velocity distribution is especially difficult at transonic velocities. Although no experimental data are available for comparison, the computed circumferential velocity distributions are shown in Figures 10 and 11 for X/D = 4.22 and X/D = 5.50, respectively. A significant asymmetry can be seen in the velocity distributions at $\phi = 90°$ and 270°. At $\phi = 90°$ cross-flow velocity caused by the angle of attack is in the same direction as the wall velocity. At $\phi = 270°$, the outer cross-flow velocity opposes the wall velocity. The circumferential velocity of profiles at $\phi = 0°$ and $\phi = 180°$ are equally affected by the surface spin. Figure 11 shows the velocity distribution at a station midway on the boattail. The circumferential velocity distribution at $\phi = 90°$ and $\phi = 270°$ has changed significantly from that shown in Figure 10. On the boattail, the decreasing body diameter results in the surface velocity decreasing in magnitude. However, the boundary-layer thickness in this region increases and the effect of surface spin is seen to persist further out.

B.   Pitch Plane and Magnus Coefficients

An integration of the pressure and viscous forces has been carried out in order to determine the aerodynamic coefficients. The sign convention used for the coefficients is shown in Figure 12. The results in Figures 13-17 are plotted as a function of longitudinal position and thus show how the force develops over the length of the projectile. Figure 13 is a plot of the normal force coefficient and shows the rapid increase in normal force which occurs on the ogive portion of the projectile. The cylinder portion should produce no significant additional normal force; however, the computation indicates a slight increase in normal force here. The reversal in the direction of the force on the boattail can be clearly seen as the accumulated normal force decreases over the length of the boattail. The experimental normal force coefficient, indicated by the circle, shows very good agreement with the computation. The spin rate of typical artillery shell is of the order of 300-500 rev/sec. As mentioned previously, the Magnus effect results from a spin-induced distortion of the viscous boundary layer which occurs for artillery shell at angle of attack. Previous studies[1,3] have shown that the Magnus effect consists of the sum of the boundary-layer displacement effect (asymmetric surface pressure distribution) plus the viscous wall shear stress contributions $\tau_x = \mu(\frac{du}{dy})_{y=0}$ and $\tau_\phi = \mu(\frac{dw}{dy})_{y=0}$. The development of all three components of the Magnus force are shown in Figures 14, 15, and 16, respectively, as a function of longitudinal position. Both the longitudinal and circumferential components (Figures 14 and 15) are seen to be of the order of 10^{-5} and 10^{-4}, respectively. The pressure component (Figure 16) is of the order 10^{-2}. The dominant component of the transonic Magnus effect is, therefore, seen to be the boundary-layer displacement effect, Cy_{p_w}. Additionally, the

largest portion of the total Magnus effect is seen to develop on the boattail where the viscous boundary layer reaches its maximum thickness. This is the

15

same qualitative behavior reported by Sturek, et al[1,3] for supersonic flow. The total Magnus force, Cy, and its components Cy_u (longitudinal shear stress), Cy_w (circumferential shear stress), and Cy_{p_w} (pressure) are shown in Figure 17. The total Magnus force can be compared with the experimental data whereas the components are shown to indicate the relative magnitude of each. Considering the small magnitude of the Magnus force and the agreement achieved for the normal force, the quantitative agreement between the computation and experiment is regarded as very good. The experimental Magnus force measurements were obtained in a wind tunnel not specifically designed for transonic flow and are considered to be of good qualitative value but of questionable quantitative value. Additional computations at various transonic Mach numbers and reliable experimental data are required before a full assessment of the computational technique can be made. This first result, however, for predicting the Magnus effect at transonic velocity is considered very encouraging.

VII. SUMMARY

The research effort presented in this paper is part of an overall program to develop a sophisticated predictive capability for projectile aerodynamics. The pacing requirement for this capability is the determination of the Magnus force in the transonic flight regime.

An implicit finite difference code, which solves the unsteady thin-layer Navier-Stokes equations, has been applied to a projectile shape at α = 2.0°, M = 0.91. The solution was marched in time until a steady-state result was obtained. Computations were first performed on a CDC 7600 using a finite difference grid of 21,600 points and required 7.78 hours of computer time. Increased grid resolution with faster computational speed per grid point was obtained by performing the computation on a Cray 1S vector computer.

The computations have been compared to experimental surface pressures and aerodynamic force coefficients. The circumferential velocity distribution, presented for two axial locations, showed the significant interaction between the cross-flow velocity resulting from angle of attack and the body-surface velocity. Experimental velocity profile data, which are very difficult to obtain for a spinning model at transonic speeds, are required to fully assess the computational results. The normal and Magnus force coefficients have been shown to be in good quantitative agreement with experimental data. The individual components of the Magnus force have additionally been presented and indicate qualitatively good results. The need for additional grid resolution or adaptive grid techniques[13] have been identified as a further requirement to achieve more accurate predictions. Good quality experimental, transonic Magnus data is also required for future code validation.

---

13. Dwyer, H.A., Kee, R.J., and Sanders, B.R., "Adaptive Grid Method for Problems in Fluid Mechanics and Heat Transfer," AIAA Journal, Vol. 18, October 1980, pp. 1205-1212.

The present results indicate that the thin-layer Navier-Stokes computational technique, in conjunction with enhanced computer technology, has the potential of providing the capability to accurately predict the aerodynamic behavior of spinning shell at transonic velocities, including the Magnus effect.

ACKNOWLEDGEMENT

PROJECTILE-TYPE BODY
(a)

X = CONST. PLANE
(b)

ϕ = CONST. PLANE
(c)
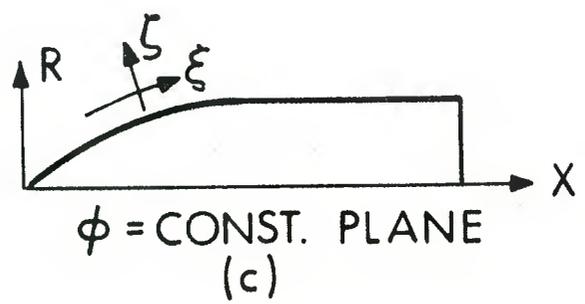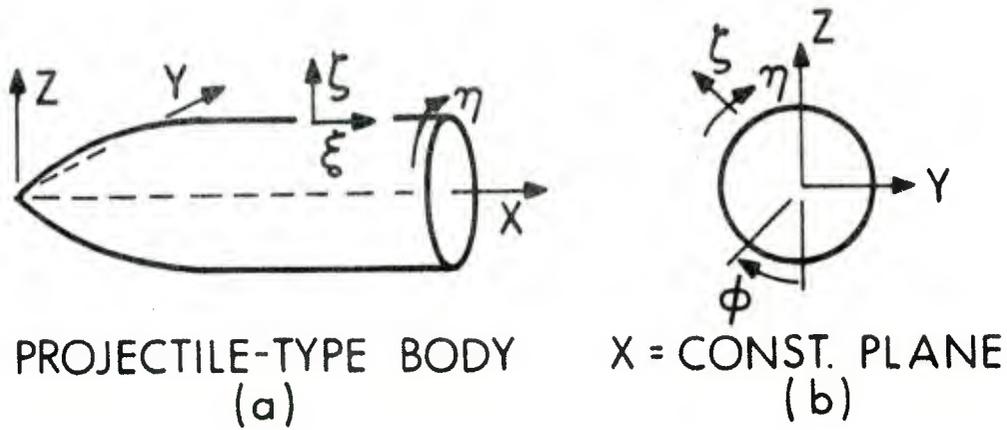
Figure 1. Physical and Transformed Coordinate System
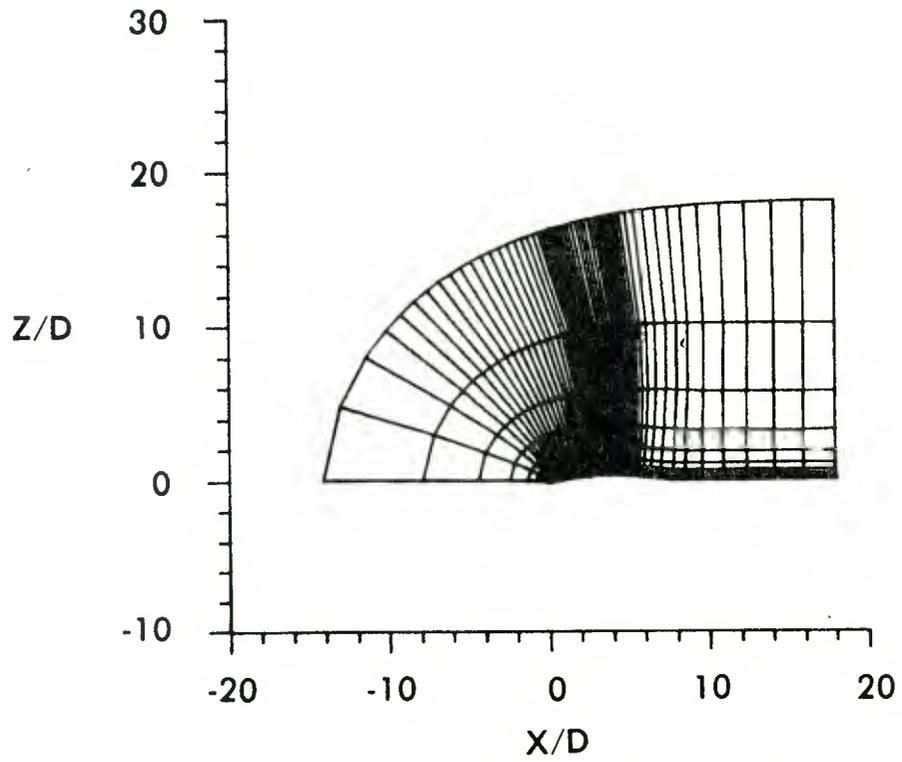

Figure 2. Physical Grid - Total Flow Field

18
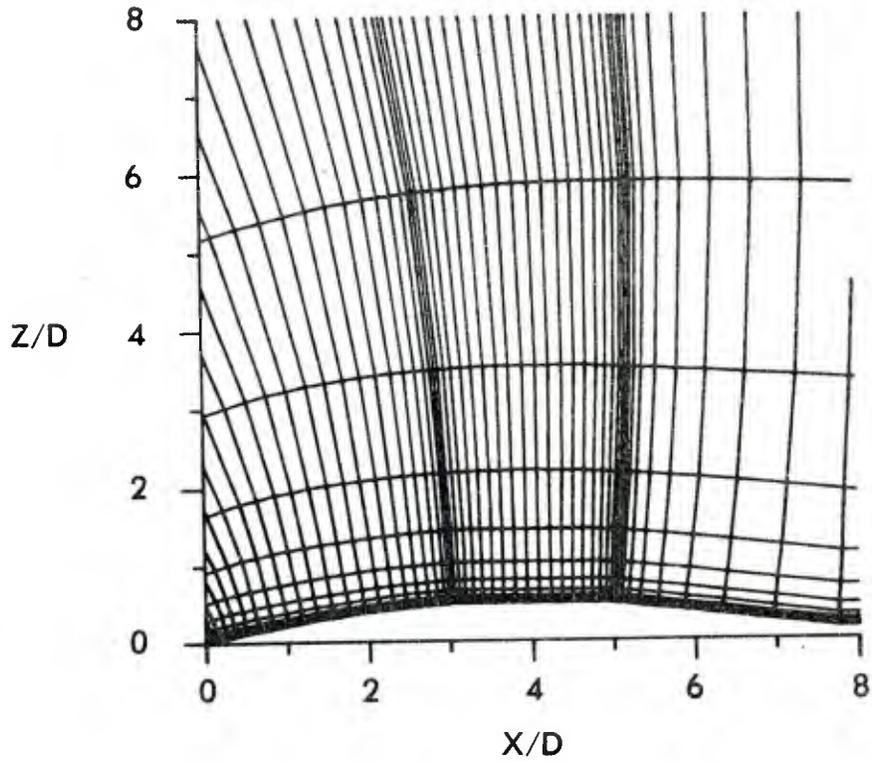
Figure 3. Physical Grid - Expanded View Near Projectile Surface
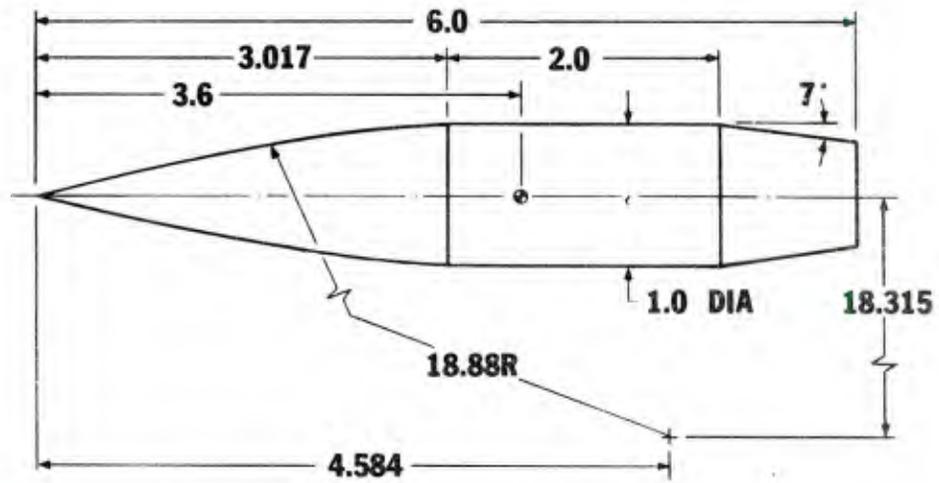
ALL DIMENSIONS IN CALIBERS
DIA = 2.25 inches

Figure 4. Model Details

19
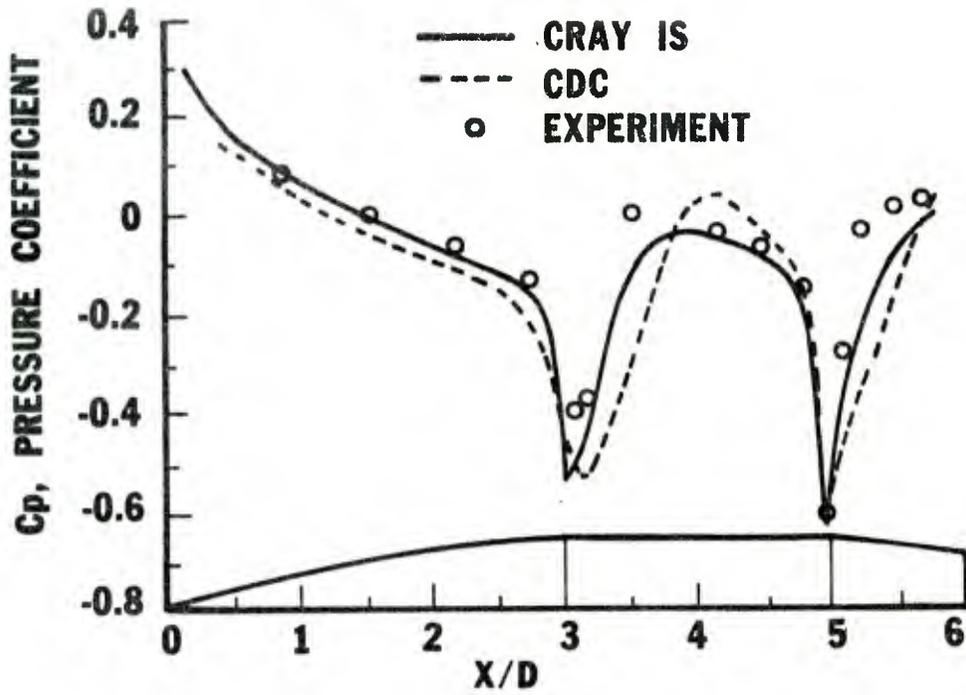
Figure 5. Surface Pressure Coefficient, Experiment and
Computations, M = 0.91, α = 2.0°
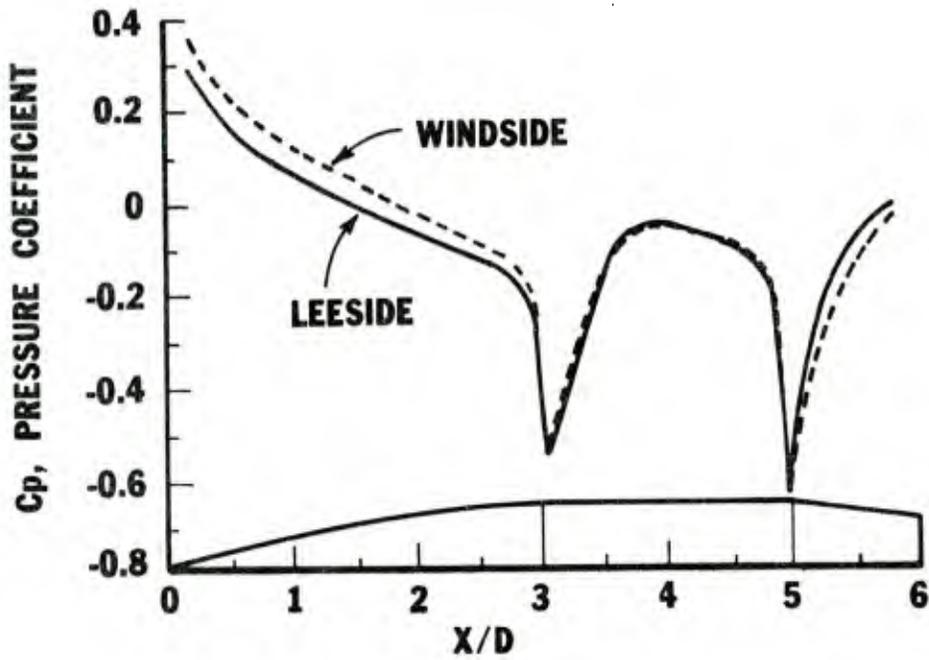

Figure 6. Windward and Leeward Surface Pressure
Coefficient, M = 0.91, α = 2.0°
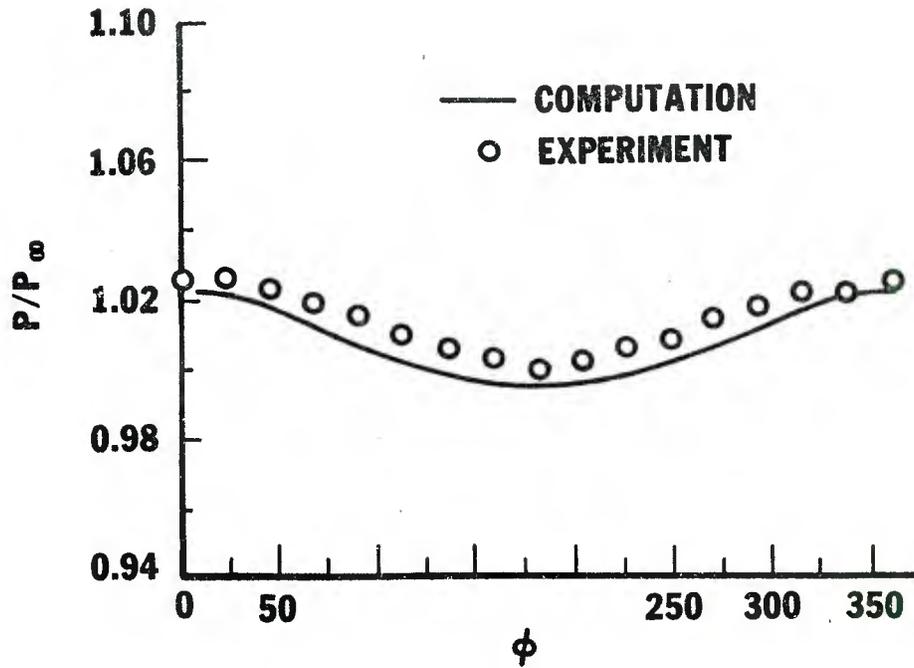
Figure 7.   Circumferential Pressure Distribution,
M = 0.91, α = 2.0°, X/D = 1.56
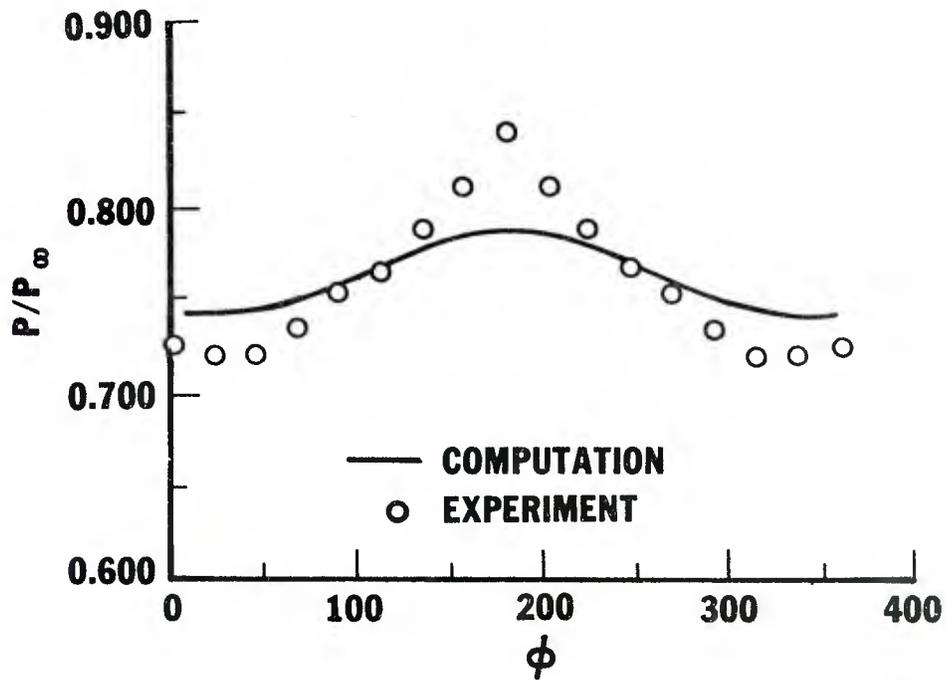
Figure 8.   Circumferential Pressure Distribution,
M = 0.91, α = 2.0°, X/D = 5.19
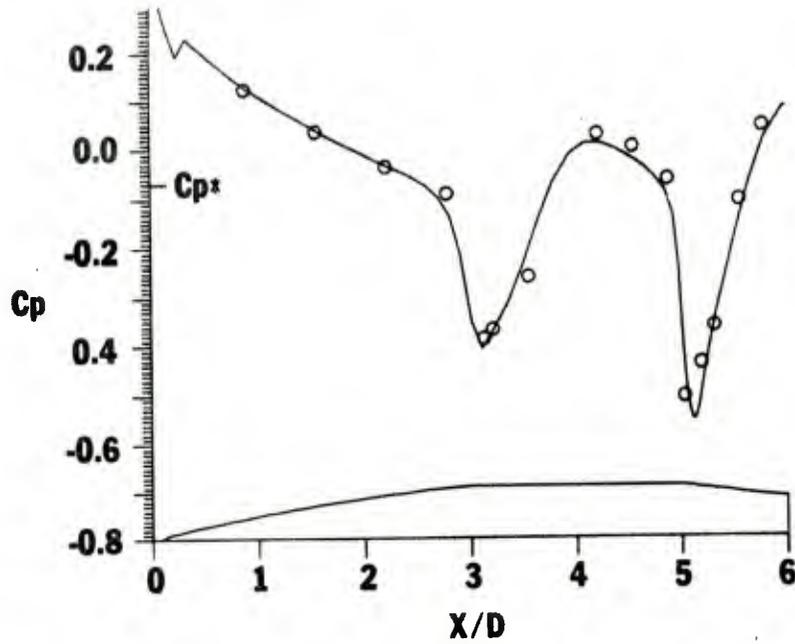
Figure 9. Surface Pressure Coefficient, Experiment and
Axisymmetric Computation, M = 0.96, α = 0.0°
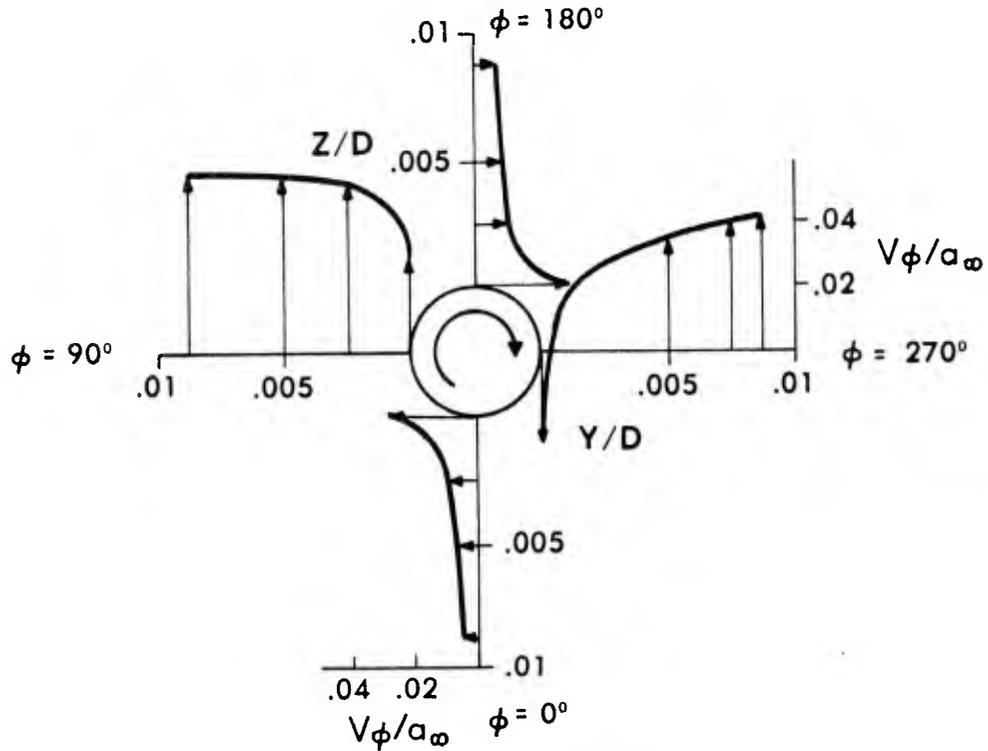
Figure 10. Circumferential Velocity Profiles for φ = 0°, 90°, 180°,
270° at M = 0.91, α = 2.0°, X/D = 4.22, PD/V = .39

22
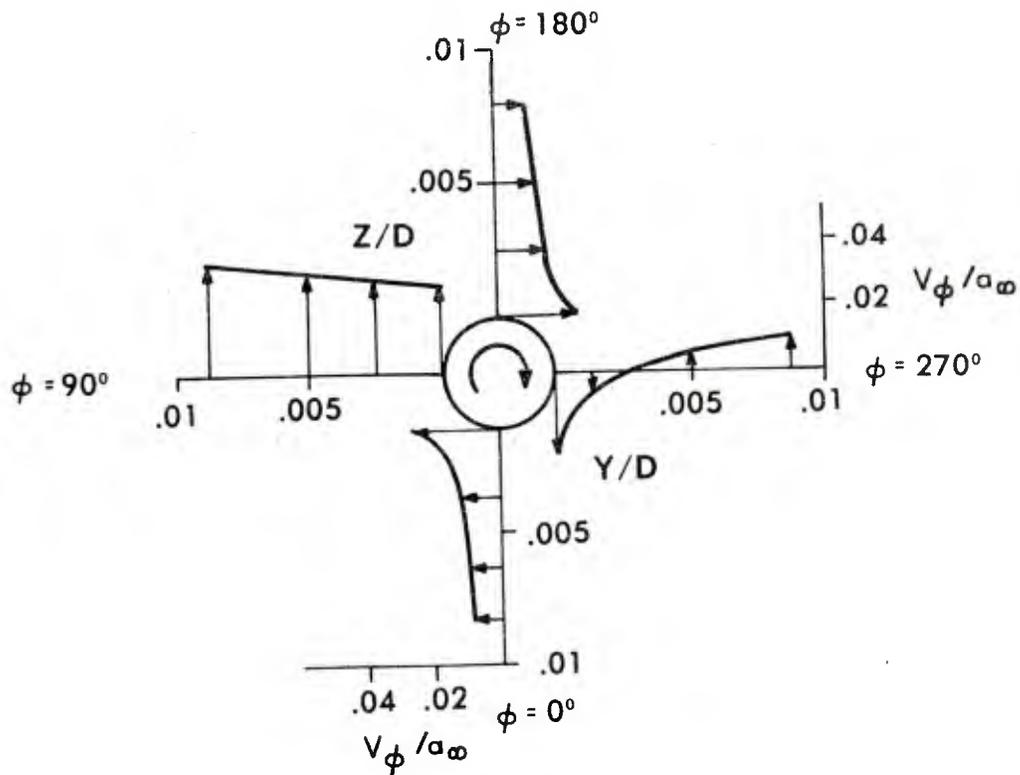
Figure 11. Circumferential Velocity Profiles for ϕ = 0°, 90°, 180°, 270° at M = 0.91, α = 2.0°, X/D = 5.5, PD/V = .39
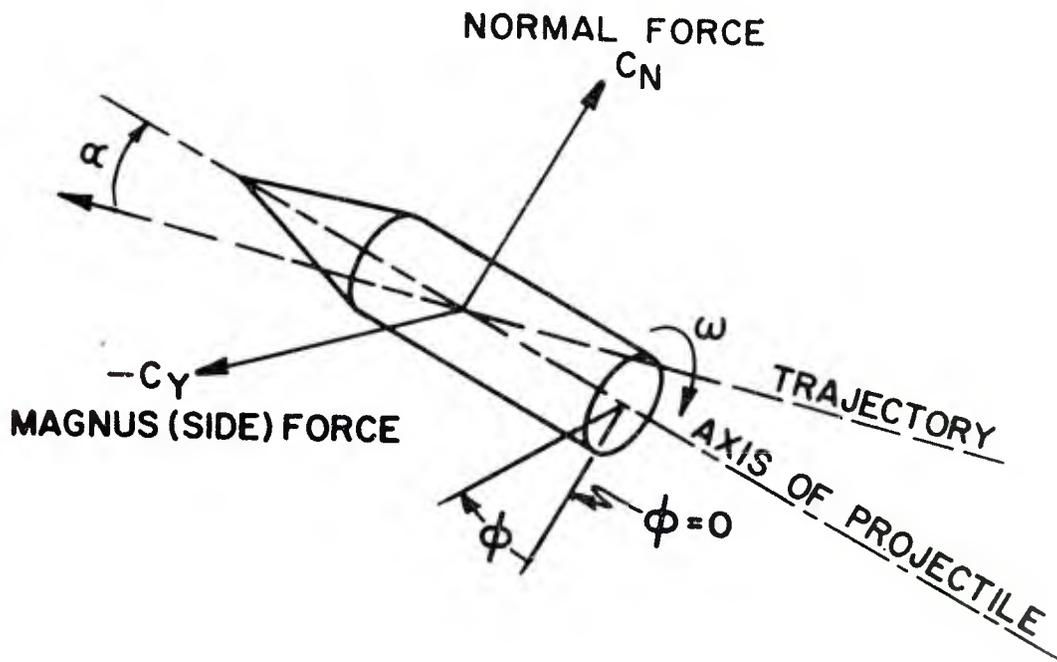
Figure 12. Aerodynamic Coefficient Sign Convention
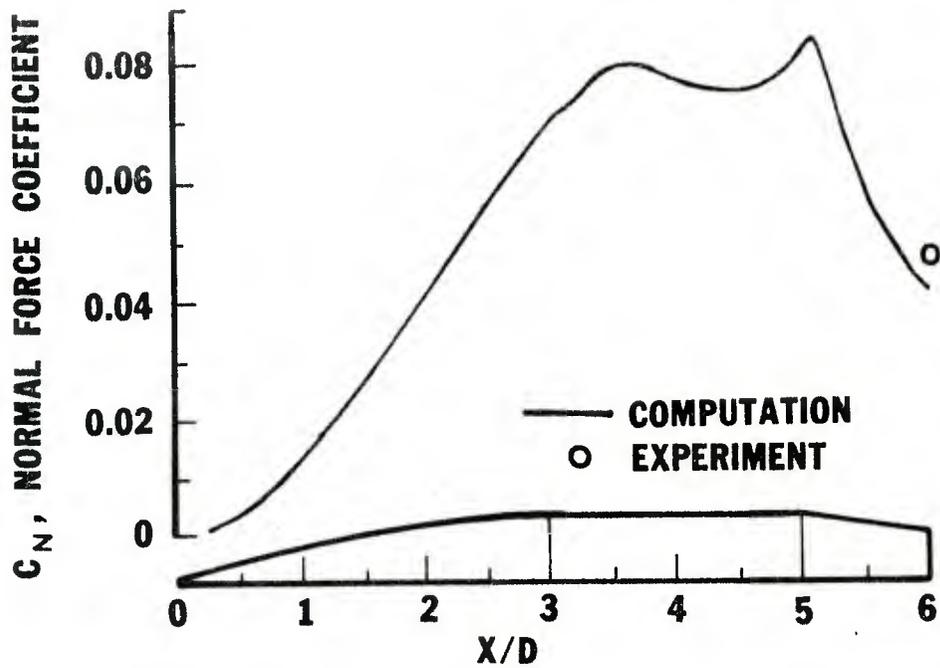
Figure 13. Normal Force Coefficient Along the Projectile, Computation and Experiment, M = 0.91, α = 2.0°
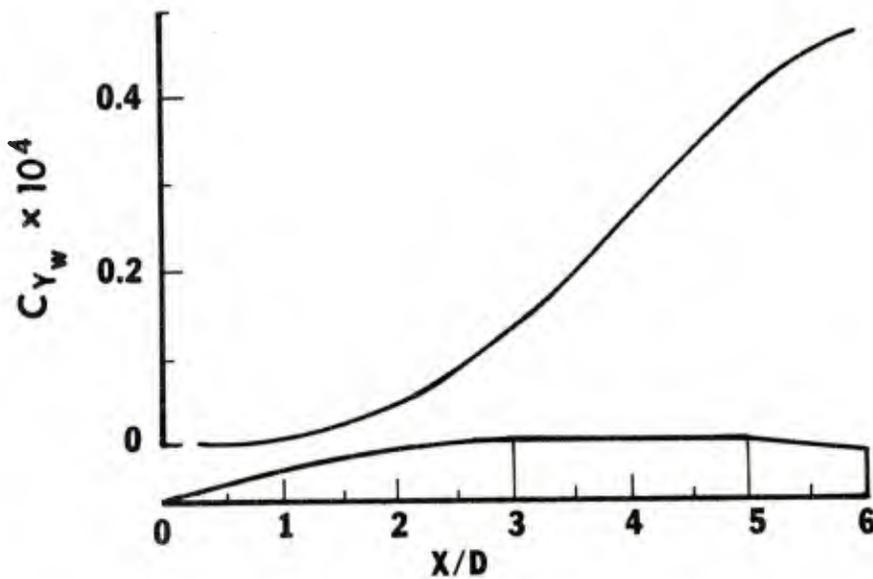
Figure 14. Circumferential Wall Shear Contribution to Magnus Force, M = 0.91, α = 2.0°, PD/V = .39
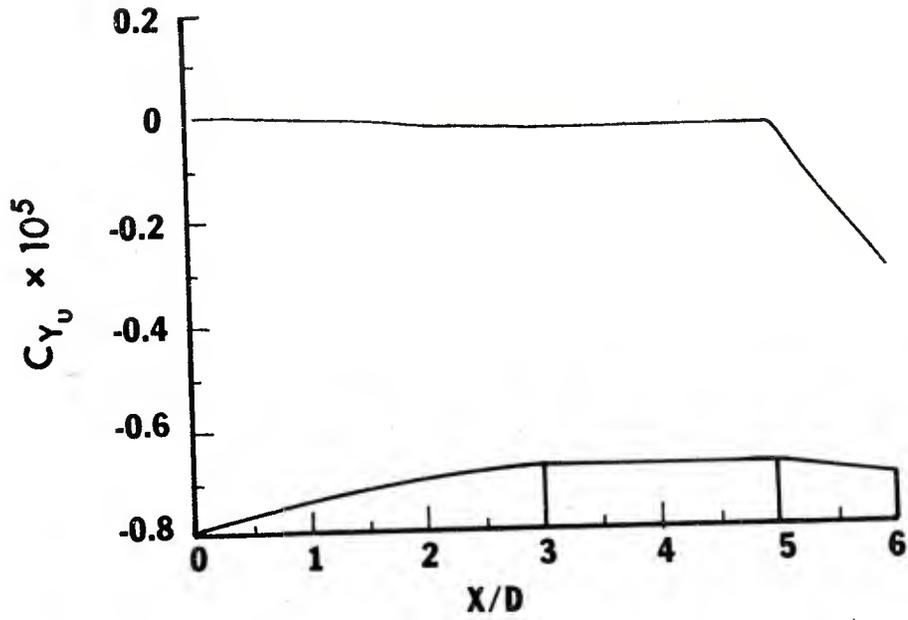
Figure 15. Longitudinal Wall Shear Contribution to the Magnus Force, M = 0.91, α = 2.0°, PD/V = .39
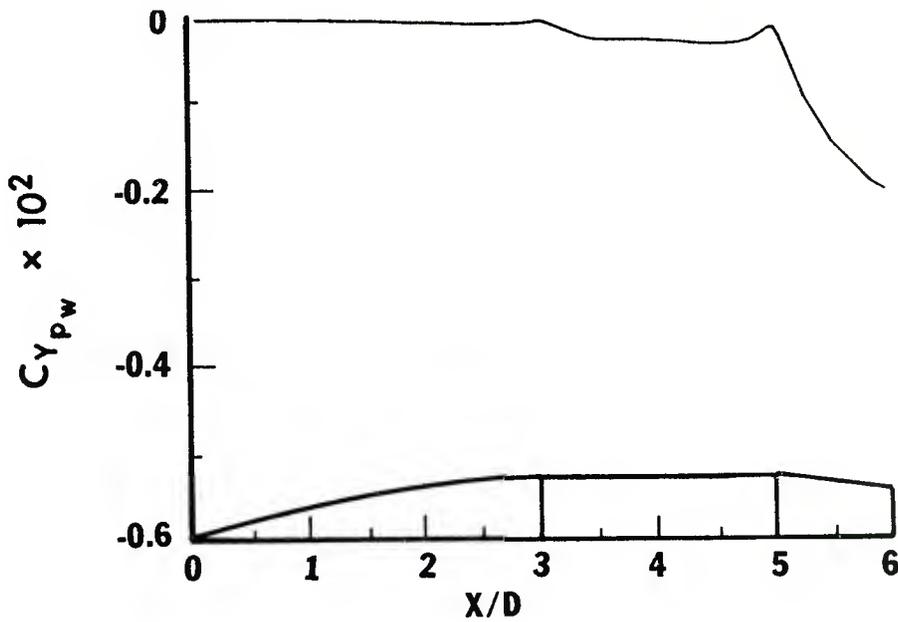
Figure 16. Pressure Contribution to the Magnus Force, M = 0.91, α = 2.0°, PD/V = .39
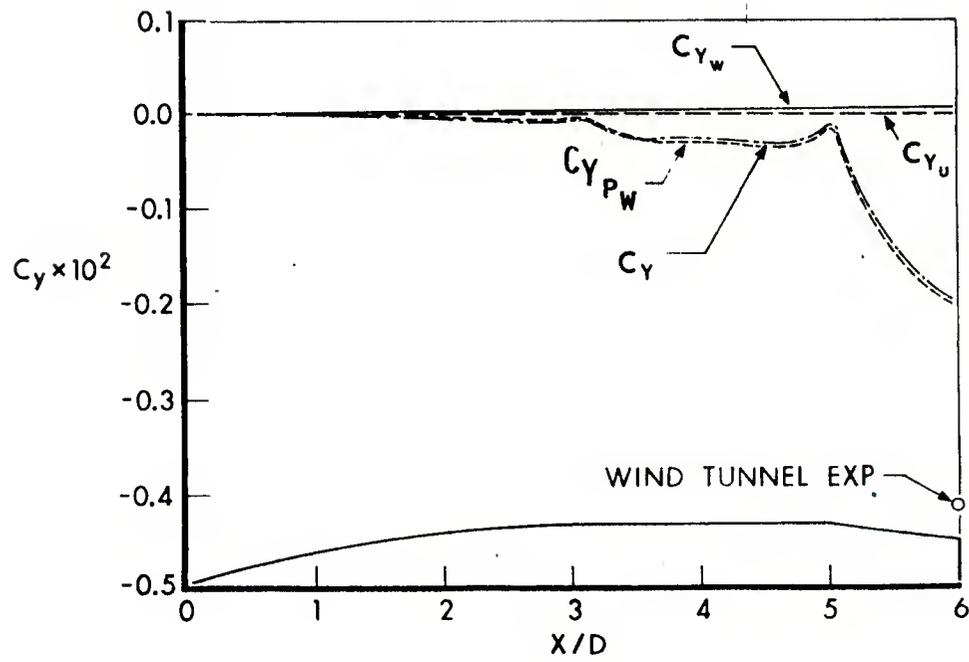
Figure 17. Magnus Components and Total Magnus Force Along Projectile, Computation and Experiment, M = 0.91, α = 2.0°, PD/V = .39

REFERENCES

1. Sturek, W.B., et al., "Computations of Magnus Effects for a Yawed, Spinning Body of Revolution," AIAA Journal, Vol. 16, No. 7, July 1978, pp. 687-692.

2. Schiff, L.B., and Sturek, W.B., "Numerical Simulation of Steady Supersonic Flow Over Cone Ogive-Cylinder-Boattail Body," AIAA Paper No. 80-0066, January 14-16, 1980; also, ARBRL-TR-02363, U.S. Army Ballistic Research Laboratory, ARRADCOM, Aberdeen Proving Ground, MD 21005, September 1981 (AD A106060).

3. Sturek, W.B., and Schiff, L.B., "Computations of the Magnus Effect for Slender Bodies in Supersonic Flow," AIAA Journal, Vol. 20, No. 12, December 1982, pp. 1724-1731.

4. Nietubicz, C.J., Pulliam, T.H., and Steger, J.L., "Numerical Solution of the Azimuthal-Invariant Thin-Layer Navier-Stokes Equations," AIAA Journal, Vol. 18, No. 12, December 1980, pp. 1411-1412.

5. Nietubicz, C.J., "Navier-Stokes Computations for Conventional and Hollow Projectile Shapes at Transonic Velocities," AIAA Paper No. 81-1262, AIAA 14th Fluid and Plasma Dynamics Conference, Palto Alto, CA, 1981; also ARBRL-MR-03184, U.S. Army Ballistic Research Laboratory, ARRADCOM, Aberdeen Proving Ground, MD 21005, July 1982 (AD A116866).

6. Deiwert, G.S., "Numerical Simulation of Three Dimensional Boattail Afterbody Flow Field," AIAA Journal, Vol. 19, No. 5, May 1981, pp. 582-588.

7. Baldwin, B.S., and Lomax, H., "Thin Layer Approximation and Algebraic Model for Separated Turbulent Flows," AIAA Paper No. 78-257, January 1978.

8. Pulliam, T.H., and Steger, J.L., "On Implicit Finite-Difference Simulations of Three-Dimensional Flow," AIAA Journal, Vol. 18, No. 2, February 1980, pp. 159-167.

9. Beam, R., and Warming, R.F., "An Implicit Factored Scheme for the Compressible Navier-Stokes Equations," AIAA Journal, Vol. 16, No. 4, April 1978, pp. 393-402.

10. Kayser, L.K., and Whiton, F., "Surface Pressure Measurements on a Boattailed Projectile Shape at Transonic Speeds," ARBRL-MR-03161, U.S. Army Ballistic Research Laboratory, ARRADCOM, Aberdeen Proving Ground, MD 21005, March 1982 (AD A113520).

11. Klopfer, G.H., and Chaussee, D.S., "Numerical Solution of Three-Dimensional Transonic Flows Around Axisymmetric Bodies at Angle of Attack," 11th Navy Symposium on Aeroballistics, Philadelphia, PA, August 22-24, 1978.

12. Kayser, L.D., Ballistic Research Laboratory/ARRADCOM, Aberdeen Proving Ground, Maryland 21005, private communications.

REFERENCES (Continued)

13. Dwyer, H.A., Kee, R.J., and Sanders, B.R., "Adaptive Grid Method for Problems in Fluid Mechanics and Heat Transfer," AIAA Journal, Vol. 18, October 1980. pp. 1205-1212.

LIST OF SYMBOLS

a	speed of sound
A	reference area, $\pi D^2/4$
c_p	specific heat (at constant pressure)
C_p	pressure coefficient
C_N	normal force coefficient, $\iint p_w \cos\phi \cos\theta_B \, dS/qA$
C_y	Magnus force coefficient, $C_{y_u} + C_{y_w} + C_{y_{p_w}}$
$C_{y_{p_w}}$	$\iint p_w \sin\phi \cos\theta_B \, dS/qA$
C_{y_u}	$\iint \tau_x \sin\phi \sin\theta_B \, dS/qA$
C_{y_w}	$\iint \tau_\phi \cos\phi \cos\theta_B \, dS/qA$
D	body diameter (57.15mm)
e	total energy per unit volume/$\rho_\infty a_\infty^2$
$\hat{E}, \hat{F}, \hat{G}, \hat{q}$	flux vector of transformed Navier-Stokes equations
J	transformation Jacobian
M	Mach number
p	pressure/$\rho_\infty a_\infty^2$
Pr	Prandtl number, $\mu_\infty c_p/\kappa_\infty$
q	free-stream dynamic pressure
R	body radius
Re	Reynolds number, $\rho_\infty D a_\infty/\mu_\infty$
Re_D	Reynolds number, $\rho_\infty D u_\infty/\mu_\infty$
S	surface area
$\hat{S}$	viscous flux vector
t	physical time
u, v, w	Cartesian velocity components/a_∞
U, V, W	Contravariant velocity components/a_∞

x,y,z	physical Cartesian coordinates
α	angle of attack
γ	ratio of specific heats
κ	coefficient of thermal conductivity/κ_∞
μ	coefficient of viscosity/μ_∞
ξ,η,ζ	transformation coordinates in axial, circumferential and radial directions
ρ	density/ρ_∞
θ_B	local body slope
τ	transformed time
τ_x	longitudinal wall shear stress
τ_ϕ	circumferential wall shear stress
ϕ	circumferential angle
ω	angular velocity, rps

Superscript

$\star$	critical value

Subscript

∞	free-stream conditions

DISTRIBUTION LIST

No. of Copies	Organization	No. of Copies	Organization

12 Administrator
Defense Technical Info Center
ATTN: DTIC-DDA
Cameron Station
Alexandria, VA 22314

1 Commander
US Army Materiel Development
and Readiness Command
ATTN: DRCDMD-ST
5001 Eisenhower Avenue
Alexandria, VA 22333

8 Commander
US Army Armament Research and
Development Command
ATTN: DRDAR-TDC
DRDAR-TSS (2 cys)
DRDAR-LCA-F
Mr. D. Mertz
Mr. A. Loeb
Mr. S. Wasserman
Mr. H. Hudgins
Mr. E. Friedman
Dover, NJ 07801

1 Commander
US Army Armament Materiel
Readiness Command
ATTN: DRSAR-LEP-L
Rock Island, IL 61299

1 Director
US Army Armament Research and
Development Command
Benet Weapons Laboratory
ATTN: DRDAR-LCB-TL
Watervliet, NY 12189

1 Commander
US Army Aviation Research and
Development Command
ATTN: DRDAV-E
4300 Goodfellow Blvd.
St. Louis, MO 63120

1 Director
US Army Air Mobility Research
and Development Laboratory
Ames Research Center
Moffett Field, CA 94035

1 Commander
US Army Communications Rsch
and Development Command
ATTN: DRSEL-ATDD
Fort Monmouth, NJ 07703

1 Commander
US Army Electronics Research
and Development Command
Technical Support Activity
ATTN: DELSD-L
Fort Monmouth, NJ 07703

2 Commander
US Army Missile Command
ATTN: DRSMI-R
DRSMI-RDK
Mr. R. Deep
Redstone Arsenal, AL 35898

1 Commander
US Army Missile Command
ATTN: DRSMI-YDL
Redstone Arsenal, AL 35898

1 Commander
US Army Tank Automotive
Command
ATTN: DRSTA-TSL
Warren, MI 48090

1 Director
US Army TRADOC Systems
Analysis Activity
ATTN: ATAA-SL
White Sands Missile Range
NM 88002

1 Commander
US Army Research Office
P. O. Box 12211
Research Triangle Park
NC 27709

DISTRIBUTION LIST

No. of Copies	Organization
1	Commander US Naval Air Systems Command ATTN: AIR-604 Washington, D. C. 20360

4	Commander
	US Naval Surface Weapons
	  Center
	ATTN: Dr. T. Clare, Code DK20
	      Dr. P. Daniels
	      Mr. D. A. Jones III
	      Mr. L. Mason
	Dahlgren, VA 22448

4	Commander
	US Naval Surface Weapons
	  Center
	ATTN: Code 312
	      Dr. C. Hsieh
	      Dr. W. Yanta
	      Mr. R. Voisinet
	      Code R44
	      Dr. R. U. Jettmar
	Silver Spring, MD 20910

1	Commander US Naval Weapons Center ATTN: Code 3431, Tech Lib China Lake, CA 93555
1	Director NASA Langley Research Center ATTN: NS-185, Tech Lib Langley Station Hampton, VA 23365
2	Commandant US Army Infantry School ATTN: ATSH-CD-CSO-OR Fort Benning, GA 31905

3	Director
	NASA Ames Research Center
	ATTN: MS-202A-14, Dr. P. Kutler
	      MS-202-1, Dr. T. Pulliam
	      MS-227-8, Dr. L. Schiff
	Moffett Field, CA 94035

No. of Copies	Organization

2	Sandia Laboratories
	ATTN: Division No. 1331,
	         Mr. H.R. Vaughn
	         Mr. G.R. Eisler
	Albuquerque, NM 87115

1	AEDC Calspan Field Services ATTN: MS 600 (Dr. John Benek) AAFS, TN 37389
1	AFWL/SUL Kirtland AFB, NM 87117
1	Stanford University Department of Aeronautics and Astronautics ATTN: Prof. J. Steger Stanford, CA 94305

1	University of California,
	  Davis
	Department of Mechanical
	  Engineering
	ATTN: Prof. H.A. Dwyer
	Davis, CA 95616

1	University of Delaware Mechanical and Aerospace Engineering Department ATTN: Dr. J. E. Danberg Newark, DE 19711

Aberdeen Proving Ground

Dir, USAMSAA
   ATTN: DRXSY-D
         DRXSY-MP, H. Cohen

Cdr, USATECOM
   ATTN: DRSTE-TO-F

Dir, USACSL, Bldg. E3516, EA
   ATTN: DRDAR-CLB-PA
         DRDAR-CLN
         DRDAR-CLJ-L

<u>USER EVALUATION OF REPORT</u>

Please take a few minutes to answer the questions below; tear out
this sheet, fold as indicated, staple or tape closed, and place
in the mail. Your comments will provide us with information for
improving future reports.

1. BRL Report Number _____

2. Does this report satisfy a need? (Comment on purpose, related
project, or other area of interest for which report will be used.)

_____

_____

_____

3. How, specifically, is the report being used? (Information
source, design data or procedure, management procedure, source of
ideas, etc.)_____

_____

_____

4. Has the information in this report led to any quantitative
savings as far as man-hours/contract dollars saved, operating costs
avoided, efficiencies achieved, etc.? If so, please elaborate.

_____

_____

5. General Comments (Indicate what you think should be changed to
make this report and future reports of this type more responsive
to your needs, more usable, improve readability, etc.)_____

_____

_____

_____

6. If you would like to be contacted by the personnel who prepared
this report to raise specific questions or discuss the topic,
please fill in the following information.

                    Name: _____

        Telephone Number: _____

Organization Address: _____

                      _____

                      _____